Tribology International 128 (2018) 104–112

Contents lists available at ScienceDirect

Tribology International

journal homepage: www.elsevier.com/locate/triboint

# Micro-tribological performance of fullerene-like carbon and carbon-nitride surfaces

F.J. Flores-Ruiz[a], M.D. Tucker[b], K.D. Bakoglidis[b,c], X. Yu[d], A.J. Gellman[d], A. Herrera-Gomez[e], L. Hultman[b], J. Rosen[b], E. Broitman[b,*,1]

[a] CONACYT-Instituto de Física, Benemérita Universidad Autónoma de Puebla, Apdo. Post. J-48, Puebla, Pue, 72570, Mexico
[b] Thin Film Physics Division, Department of Physics, Chemistry and Biology (IFM), Linköping University, SE-58183, Linkoping, Sweden
[c] School of Materials, Faculty of Science and Engineering, The University of Manchester, M13 9PL, Manchester, United Kingdom
[d] Department of Chemical Engineering, Carnegie Mellon University, Pittsburgh, PA 15213, USA
[e] CINVESTAV-Unidad Queretaro, Queretaro, Qro, 76230, Mexico

ARTICLE INFO

*Keywords:*
Fullerene-like films
Microtribology
Carbon-nitride films
Carbon films

ABSTRACT

We studied the microtribological behavior of amorphous and fullerene-like (FL) carbon and carbon-nitride coatings deposited by filtered-cathodic-arc. All films show similar friction coefficients but different wear mechanisms. The FL films exhibit a surface swelling with the formation of a layer that thickens during the test, limiting wear and maintaining a low friction. X-ray photoelectron spectroscopy on worn FL film surfaces show an increase in the sp$^2$-content, indicating that the lubricious layer generated by the wear process is probably the result of re-hybridization due to plasticity induced by localized shear. In contrast, the wear results of the amorphous films, involving tribomechanical and tribochemical surface phenomena, show that the surface layer formed during sliding is a precursor to the onset of wear.

## 1. Introduction

Fullerene-like carbon (FLC) and carbon nitride (FL-CN$_x$) films are perhaps the next generation of solid lubricants. They have outstanding mechanical and tribological properties, with hardness and modulus comparable to TiN coatings, one of the most well-known and studied industrial coatings [1]. However, the much lower friction coefficient and superior resistance to wear of FL films [1] makes them suitable for potential applications ranging from biomedicine [2] to aerospace [3]. A feature of FL-CN$_x$ films is their high hardness and elasticity due to the nitrogen which incorporates into the graphitic microstructure to form pentagonal rings inducing curvature, and promoting cross-linking of graphite planes [4,5,6]. In the case of FLC films, their microstructure contains *graphitic carbon nanoparticles* such as nanotubes and onion-like formations linked to the tetrahedral amorphous carbon (ta-C) network by sp$^3$-bonds [7].

Despite the extensive mechanical and tribological research on FLC over the past two decades, some tribological questions remain unanswered. One of these questions concerns the mechanism that yields the low friction coefficient and low wear rate observed during friction-wear tests at the micro- or nano-scale. To begin to understand these new materials, it is necessary to analyze the knowledge gained from prior study of ta-C or hydrogen-free diamond-like carbon (DLC) films. Voevodin *et al.* studied the macro-tribological behavior of 0.5-µm-thick DLC coatings sliding against sapphire and steel balls using a ball-on-disk configuration at 50% relative humidity (RH) [8]. By Raman analysis of the wear track, they observed an amorphous carbon layer (sp$^2$-rich carbon hybridization) formed at the sliding interface by tribo-thermal and tribo-mechanical processes induced by shear stresses. This sp$^2$-rich layer was responsible for the low friction and wear of DLC coatings. These results were similar to those found by Erdemir *et al.* [9,10] for wear tracks on H-DLC analyzed by Fourier transform infrared and Raman spectroscopy [8]. Later, Tambe and Bhushan carried out nanotribological experiments on hydrogen-free DLC films with an atomic force microscope (AFM) working at 50% RH [11]. Using the instrument in friction mode with the AFM-tip operating as a single asperity in contact with the DLC surface, they tried to determine whether a transformation from sp$^3$ to sp$^2$ was the cause of the low friction and wear observed at nanoscale. Their results agree with the suggestions by Voevodin and Erdemir that the low shear strength of a single a-C layer formed during the sliding is responsible for the good tribological behavior observed for DLC. This tribolayer formed after

---

[*] Corresponding author.
*E-mail address:* esteban.daniel.broitman@skf.com (E. Broitman).
[1] Present address: SKF Research & Technology Development Center, 3439 MT Nieuwegein, Netherlands.

https://doi.org/10.1016/j.triboint.2018.07.009
Received 1 January 2018; Received in revised form 10 May 2018; Accepted 5 July 2018

**Table 1**
Mechanical properties of carbon and carbon nitride films grown at different substrate temperatures and nitrogen pressure [25]. The coatings having a fullerene-like structure are indicated with FL.

| Substrate Tempera-ture $T_S$ (°C) | $N_2$ Pressure (mTorr) | Structure | Hardness (GPa) | Reduced Elastic Modulus (GPa) | Initial mean Hertzian pressure (GPa) | Plasticity index $H^3/E^2$ | Elastic Recovery (%) |
|---|---|---|---|---|---|---|---|
| | 0 | – | 48.8 ± 2.2 | 344 ± 5 | 11.00 | 0.982 | 95 |
| 20 | 0.5 | – | 29.6 ± 0.4 | 249 ± 8 | 8.85 | 0.418 | 86 |
| | 5 | – | 13.3 ± 0.2 | 142 ± 3 | 6.08 | 0.116 | 68 |
| | 0 | FL | 21.8 ± 0.4 | 182 ± 5 | 7.18 | 0.312 | 94 |
| 300 | 0.5 | FL | 17.0 ± 0.4 | 145 ± 1 | 6.17 | 0.237 | 92 |
| | 5 | – | 8.3 ± 0.1 | 76 ± 1 | 4.01 | 0.099 | 84 |

sliding was also observed at the macroscale by Joly-Pottutz et al. for H-free and hydrogenated DLC coatings lubricated with glycerol; a 50 nm thick tribolayer on the sliding track was correlated to a $sp^3 \rightarrow sp^2$ transformation [12]. Later, an experimental quantification of the $sp^3$ to $sp^2$ phase transformation at the nanoscale induced by an *in situ* transmission electron microscopy sliding experiment was reported by Marks *et al.* [13,14]. They found that the rate of phase transformation under their experimental conditions is about 0.018% transformed volume per sliding pass with a thickness increase in the top layer.

Analysis of tribocoupled systems with molecular dynamic (MD) simulations has shown that a shear localization mechanism and the formation of an amorphous carbon (a-C) tribolayer is responsible for the low friction observed in carbon-based materials [15]. The reorientation of the C-C bonds towards the sliding direction and a possible clustering of graphene-like sheets characterize this mechanism. Similar simulation studies by Pastewka *et al.*, but on tribocoupled systems of diamond [16], revealed a transformation from $sp^3$ to $sp^2$ where a mechanochemical mechanism is responsible for the low friction and wear observed on the diamond surfaces. In additional, those results showed that an amorphous layer grows at the sliding interface, as the result of an $sp^3$ to $sp^2$ transition producing a carbon layer at the surface with a higher $sp^2$-hybridization fraction than in the diamond bulk. Afterwards, the same group performed experimental and MD studies in which they demonstrated that sliding induced the formation of an a-C layer on ta-C coatings with increased $sp^2$ content [17]. Their results lead them to conclude that, for tribocoupled ta-C/ta-C systems, rehybridization is dominated more by tribomechanical plasticity events induced by localized shear than by tribothermal processes (i.e., heat-induced structural transformations). These plasticity events weaken the top-most layers of ta-C due to shear-induced force-fluctuation that is carried by strong bonds in the amorphous network and break its weak bonds [17]. These oscillating forces could be consequence of a non-homogeneous distribution of hybridization states for ta-C coatings, which have been observed in nanoscale contact mechanics situations at amorphous materials such as ta-C [18] and vitreous metallic glasses [19,20].

In the particular case of FL-$CN_x$ materials, research at the macroscale indicates that a thick transfer film initially acts as a precursor to wear but, after a certain number of sliding cycles, this transfer film isolates the probe and the track, and provides a steady friction coefficient which also decreases the wear [4,21]. A similar performance has been observed in ta-C coatings [22,23]. In these studies the transfer film acts as a lubricant and provides a low and stable friction coefficient while also decreasing the wear. At the nanoscale, it has been observed that FL-$CN_X$ has a lower friction coefficient than amorphous $CN_X$ under ambient conditions, indicating that the film structure also plays a crucial role in the friction behavior [5].

In this work, we investigate the wear mechanisms acting during a linear reciprocating experiment at the microscale on amorphous and FL films of carbon and carbon nitride deposited by the filtered cathodic arc method. A method for simultaneous *in-situ* measurement of the wear and friction evolution, previously reported by some of the authors [24], was employed to allow for a quantitative comparison between the FL and amorphous structures of the carbon and carbon nitride films. The results show that both, tribomechanical (i.e., re-hybridization [17]) and tribochemical (i.e., surface passivation phenomena [23]) mechanisms, occurred depending on material's microstructure (amorphous or FL) and mechanical properties.

## 2. Experimental details

### 2.1. Film processing

Carbon and carbon nitride films with amorphous and FL structures were deposited on Si(001) substrates using a pulsed filtered cathodic arc. The chamber base pressure was $\sim 1 \times 10^{-6}$ Torr. The arc was operated using a graphite cathode with a peak current of 1.8 kA giving a growth rate of 0.083 nm/pulse for carbon films and 0.029 nm/pulse for carbon nitride films. For carbon nitride deposition, $N_2$ gas was introduced into the chamber through a mass flow controller and the total pressure was regulated with an automatic throttle valve. All films were deposited with 5000 arc pulses. The experimental details concerning the deposition, structure and mechanical properties were previously reported [25]. In this paper we analyze films deposited at the chamber base pressure of $\sim 1 \times 10^{-6}$ Torr (labeled $P_{N2} = 0$ mTorr) and with $P_{N2} = 0.5$ and 5 mTorr ($\sim 1 \times 10^{-4}$, 0.07 and 0.7 Pa, respectively). The substrate temperature was either $T_S = 20$ °C or 300 °C.

### 2.2. Friction coefficient and wear measurements

The mechanical properties of the films deposited with $P_{N2} = 0$, 0.5 and 5 mTorr at $T_S = 20$ °C and 300 °C analyzed in this study were previously reported in Ref. [25], and are presented in Table 1. Nanoindentation hardness, reduced elastic modulus, and elastic recovery were measured by using the method of Oliver and Pharr, and taking into consideration all necessary precautions about the nanomechanical characterization of thin films [26].

The microtribological tests were performed with a Triboindenter TI 950 from Hysitron operating with a conical diamond tip (60° opening angle and ~5.02 μm tip radius) moving at a speed of 1 μm/s at room temperature of ~23 °C and a relative humidity (RH) of ~50%. To produce wear, the probe makes passes with a length of 5 μm, which are repeated 31 times. The applied load during the wear-friction experiment was 5 mN, which corresponds to an initial mean Hertzian contact pressure of between 4 and 11 GPa depending on the elastic modulus of each sample (see Table 1).

The microtribological measurements were carried out by using the method for simultaneous *in-situ* friction and wear characterization [24]. The instrument head of the Triboindenter is a three-plate capacitive transducer that works as both actuator and sensor, allowing access to topographical information of less than 1 nm with a high load precision [27]. In addition, this method takes into account the thermal drift from the topographic profiles to get a good estimate of the wear rate. The roughness average ($R_a$) value is evaluated from the wear track of the topographic profiles (see equation (2) in Ref. [24]). These controls make possible the quantitative assessment of temporal evolution of the tribological data. Technical details and applications of the

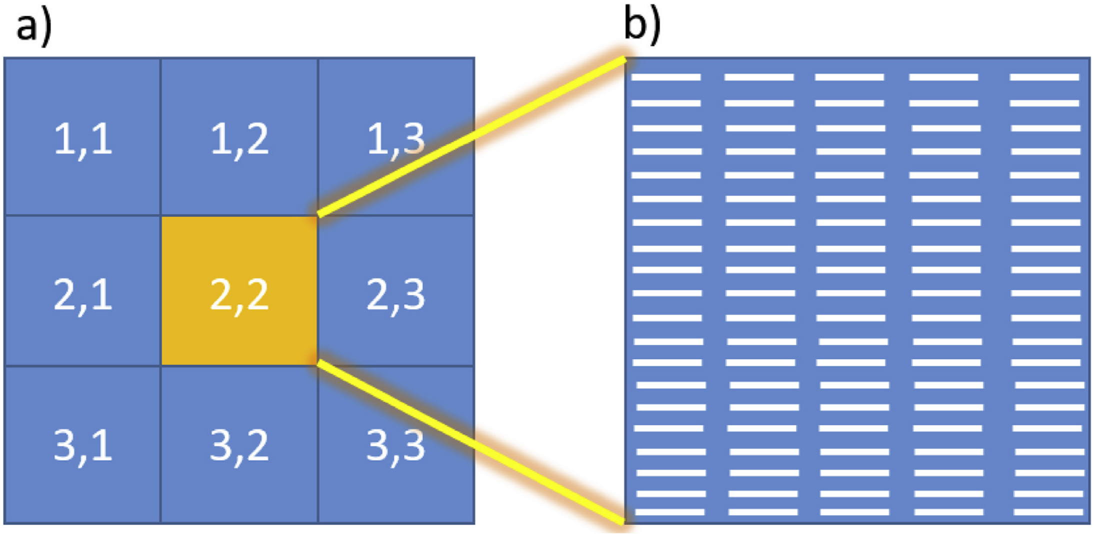

**Fig. 1.** (Color online) a) Scheme of XPS experiments carried out on the films deposited at $P_{N2} = 0$ and 0.5 mTorr and $T_S = 300\,^{\circ}C$. Spectra were obtained on nine locations labeled (i,j). The area of each location is about 60 × 60 μm$^2$; b) Location (2,2) contains 150 wear tracks of 10 μm length each. Assuming a width of the wear track of 1 μm, we obtain a percentage of worn area of ~42% [worn area (%) = (1 μm × 10 μm × 150 experiments) × 100/(60 μm × 60 μm)]. (For interpretation of the references to color in this figure legend, the reader is referred to the Web version of this article.)

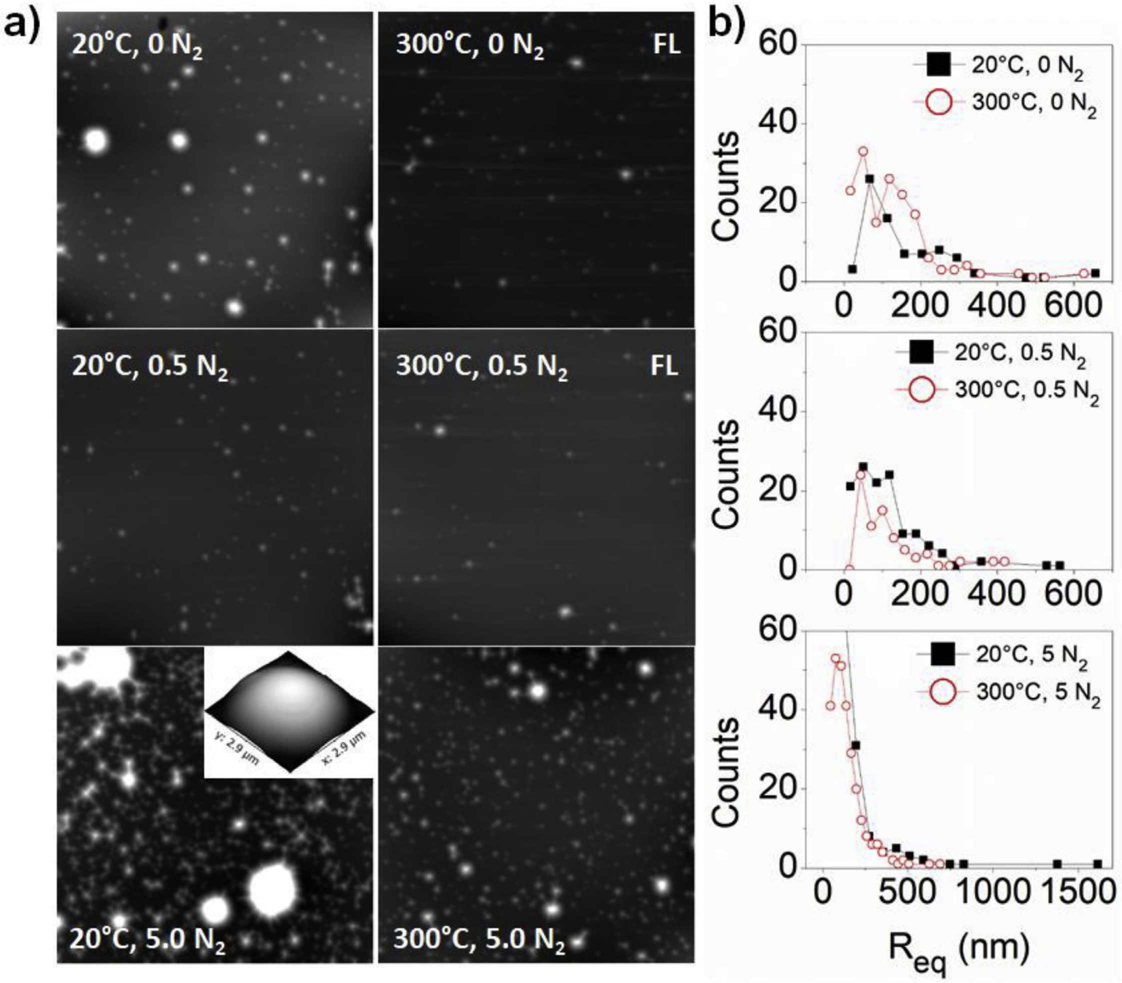

**Fig. 2.** (Color online) a) Topography SPM images obtained over 15 μm × 15 μm. The images were corrected with the blind estimation algorithm [38,39] to avoid overestimations of the particle size presented in (b). The inset in (a) shows the indenter-end reconstruction. The load applied on the indenter tip to acquire the SPM images was 2 μN. The images indicate that the coating has a fullerene-like structure. (For interpretation of the references to colour in this figure legend, the reader is referred to the Web version of this article.)

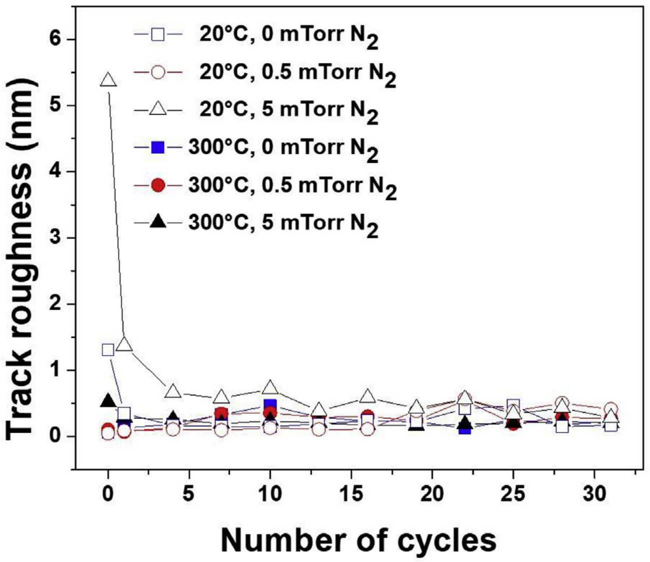

**Fig. 3.** (Color online) Evolution of the track roughness as a function of number of probe cycles. (For interpretation of the references to colour in this figure legend, the reader is referred to the Web version of this article.)

measurement method have been published elsewhere [24,28–30]. The Triboindenter instrument was also used to produce surface probe microscopy (SPM) images using the same diamond tip utilized in the microtribological tests.

### 2.3. XPS analysis of unworn and worn surfaces

X-ray photoelectron microscopy (XPS) analysis (ThetaProbe™ from ThermoFisher) was used on the virgin and worn surfaces of the films deposited at $P_{N2}$ = 0 and 0.5 mTorr and $T_S$ = 300 °C to study changes in their structure ($sp^2$ or $sp^3$) due to sliding wear of the probe. XPS experiments were carried out on nine locations labeled (i,j) as described in Fig. 1a. Location (2,2) in this figure corresponds to the worn surface. 150 wear experiments were performed on this location as is schematized in Fig. 1b. A monochromated Al Kα x-ray source (1486.6 eV) was focused to a ~50 µm diameter beam spot size. The parameters for acquisition of the spectra were 10 eV pass energy, 10 ms dwell time, 0.05 eV steps, and totals of 200 scans for C1s and N1s and 70 scans for O1s. Analysis of the XPS C1s core level spectra was executed by simultaneously peak-fitting [31,32], allowing a reliable estimation of the different contributions to the spectra [5,18]. It has been demonstrated that, with this method, it is possible to identify the centers and widths of the different peaks found in amorphous carbon [32,33]. Voigt line shapes and the Shirley background subtraction method were used during the fitting with the AAnalyzer software [34]. This software also allows estimating the uncertainties in the parameters extracted from the spectra; the method accounts for the covariance of the reported variables with all other free variables, including the parameters that determine the background signal [35,36].

## 3. Results and discussion

The amorphous or fullerene-like nature of the films was revealed by plan view TEM images and radial averages of the electron diffraction patterns (see Figs. 3 and 4 in Ref. [25]). Only the films deposited with $P_{N2}$ = 0 and 0.5 mTorr at 300 °C present FL structures while the other coatings have amorphous structures. The friction coefficient values for all films presented in this work are between 0.06 and 0.07, which is comparable to the values reported in tribological tests conducted at the macroscale [23,37], and slightly higher than values reported at the nanoscale under similar environmental conditions [5]. Due to the similarities of the friction in all samples, all our tribological results are discussed in terms of wear behavior.

### 3.1. Surface morphology

Fig. 2a shows 15 µm × 15 µm topographic scanning probe microscopy (SPM) images that allow observation of particles of different dimensions on surface of the films. Although the deposition system is filtered, it does not completely prevent the incorporation of particles (originating at the graphite cathode) into the growing film. These particles can undergo multiple reflections, leading to the formation of sub-particles due to fractures, which can be transported by the plasma via momentum exchanged with ions, thus having a significant likelihood of reaching the substrate [40]. Drescher *et al.* [41] showed that these particles are the top of "nodules" that grow on top of much smaller particles. Their model shows that such nodules grow on the film with a cone-like geometry, rather than landing fully-formed. These cone-like nodules have a graphitic nucleus at the bottom and a diamond-like structure on the top. Grain analysis by edge detection [42] of the images in Fig. 1b indicates that, under the same $N_2$ partial pressure, the films deposited at $T_S$ = 300 °C have a particle equivalent radius ($R_{eq}$) lower than films deposited at 20 °C, because of their higher thermal mobility due to the higher deposition temperature. On the other hand, films deposited at $P_{N2}$ = 5 mTorr show a considerably higher $R_{eq}$ than those films deposited at $P_{N2}$ = 0 and 0.5 mTorr, and some particles have a $R_{eq}$ > 1000 nm when $T_S$ = 20 °C. This behavior is probably due to the energy loss of carbon particles in the plasma by collisions with nitrogen species.

### 3.2. Analysis of roughness and wear

Fig. 3 shows the evolution of the track roughness as a function of the number of probe cycles. The initial track roughness for the film deposited at $T_S$ = 20 °C (higher than those for films deposited at $T_S$ = 300 °C under the same $P_{N2}$) indicates that the surface atomic mobility at the higher $T_S$ leads to a relaxed surface. Note that this initial track roughness depends on the probe position on the sample surface, however, the roughness values follow the surface morphology observed in Fig. 1a (a similar behavior has already been described for carbon nitride thin films deposited by HiPIMS [43]). As noted in the surface morphology section, the nodules resulting from incorporation of particles from the target produce changes in roughness but they are almost completely removed during the first friction-wear cycles due to the high-applied force, as is visually confirmed in the wear evolution maps presented in Fig. 4. This produced a smoother or unchanged track in comparison with the initial track as observed in Fig. 3.

In addition to roughness, the wear evolution maps (Fig. 4) show the evolution of the sample surfaces with sequential probe passes. Amorphous films deposited at $T_S$ = 20 °C with $P_{N2}$ = 0 and 0.5 (Fig. 4a and b, respectively) show a similar behavior in wear: i) during the passes 1–7, instead of wear, a layer of material swells during sliding of the tip reaching a maximum additional thickness of 2 nm for the $P_{N2}$ = 0 films and < 1 nm for the $P_{N2}$ = 0.5 film; ii) this material layer is dragged towards the track edges during passes 8–13, and subsequently acts as a wear precursor (in agreement with previous reports [17,21]); iii) finally, for passes 14–31, wear due to an abrasive or chemical process appears with depth values of < 1 nm for the $P_{N2}$ = 0 film and ~3 nm for the $P_{N2}$ = 0.5 mTorr $N_2$ film. The high hardness of these films (49 and 30 GPa for $P_{N2}$ = 0 and 0.5 mTorr, respectively) contributes to the low wear rate observed. The phenomenon of a local swelling, manifested as apparent layer growth in the beginning of the experiment, is in agreement with the experimental and simulation results reported for diamond [16], nanocrystalline diamond [44], and diamond-like carbon [12,17] coatings under contact pressures in the range 0.3–5.0 GPa.

FL films deposited at $T_S$ = 300 °C with $P_{N2}$ = 0 and 0.5 mTorr (Figure 4d and e respectively) also present interesting behavior during

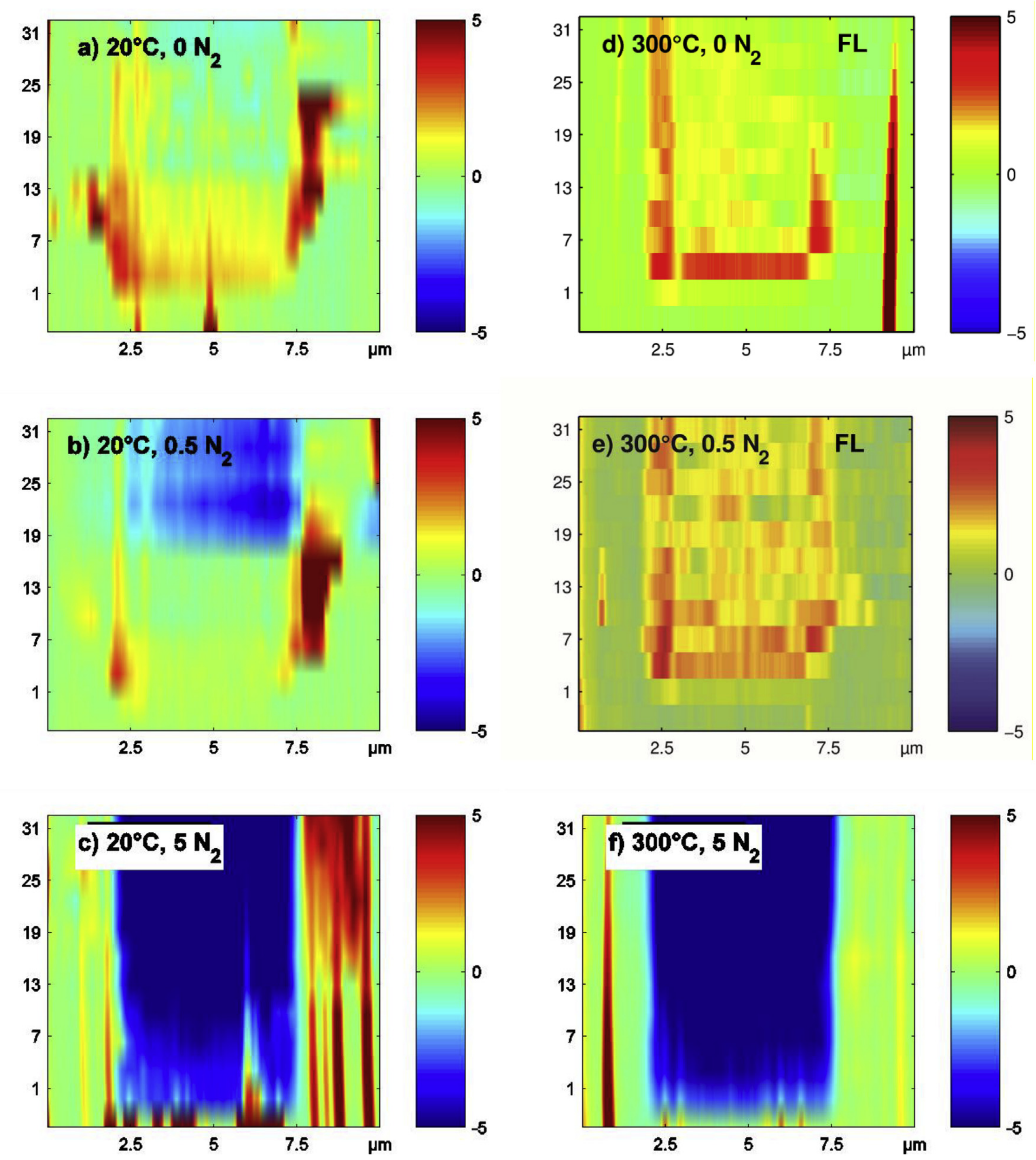

**Fig. 4.** (Color online) Wear evolution maps for films with $T_S = 20\,^{\circ}C$ (a, b and c) and $300\,^{\circ}C$ (d, e and f) at $P_{N2} = 0$, 0.5 and 5 mTorr. The y-axis indicates the number of passes, and the x-axis is the width of exploration and the scale bar represents the wear depth in nanometers (negative values indicate wear). A load of 5 mN was used to produce wear. (For interpretation of the references to colour in this figure legend, the reader is referred to the Web version of this article.)

the wear test. Their wear tracks show negative wear (i.e., local swelling of material surface) for the first thirteen passes with excess thicknesses of ~3–4 nm, indicating the formation of a layer in the sliding interface probably induced by local plasticity events, similar to the phenomena described by Kunze et al. [17]. This has already been discussed in the introduction section. In this case, the top layer (formed by local swelling) does not follow the behavior previously described for the films deposited at $T_S = 20\,^{\circ}C$ with $P_{N2} = 0$ and 0.5 mTorr, i.e., that the material layer is the precursor to wear, since the experimental result reveals a continuously expanding material layer. The results in Fig. 4d and e could obey a cyclical phenomenon, i.e., when the top layer is apparently worn off (as is observed in the track borders) the surface layer is recovered. Such cyclical phenomenon also would explain the low wear rate of fullerene-like structures observed for large sliding distances at the macroscale [4,45]. The cyclical phenomenon is controlled principally by a tribomechanical process due to plasticity events induced by localized shear as discussed in Ref. [17], but in our case, the good mechanical properties of the FL structure (hardness above 16 GPa and elastic recovery higher than 90%) allows an anelastic behavior [46] of the bulk while the surface presents a lower shear resistance than the amorphous films deposited at $T_S = 20\,^{\circ}C$ with $P_{N2} = 0$ and 0.5 mTorr. In addition, the low average roughness in the track during the start of the wear test helps observation of the low wear behavior because it prevents tip-asperity interactions that could lead to surface material peel-off, which would contribute to wear. Further tribological tests done in our samples under the same conditions have confirmed the repeatability of the swelling phenomena.

Since the wear behavior of the amorphous ($T_S = 20\,^{\circ}C$) and FL ($T_S = 300\,^{\circ}C$) material deposited with $P_{N2} = 0$ and 0.5 mTorr is considerably different, it is clear that the material structure plays an important role. The top layer formed during sliding can contain structural similarities to the bulk from which it was removed, but also, its interaction with the humidity of the surroundings should be considered. For the case of amorphous surfaces, previous studies have shown that they have a water adsorption level higher than FL surfaces, which means that the amorphous surfaces have a high concentration of unsaturated bonds that can be rapidly passivated [47]. Konicek *et al.* [23] have estimated that an unterminated diamond (111) surface exposed to 1% RH and ambient temperature, where ideally every $H_2O$ molecule is dissociated, takes around $2.5 \times 10^{-5}$ s to become fully passivated. For the case of FL surfaces, density functional theory studies have shown that the energy cost for dangling bond formation is 1.34–1.39 eV, about ~2.9 and ~2.5 times higher than for amorphous carbon and carbon nitride materials, which means less probability of material interaction with water molecules [45]. Based on the above, surfaces with the FL structure are less likely than amorphous surfaces to react with ambient moisture during the sliding, which leads us to conclude that the process leading to thickening of the surface layer is predominantly tribomechanical rather than tribochemical.

Amorphous films grown at $P_{N2}$ = 5 mTorr and $T_S$ = 20 and 300 °C (Fig. 4c and f, respectively) exhibit the highest wear depth values (~5 nm). Here, the passivation phenomenon [23] is dominant during the wear-friction experiment since the wear produced by the tip is the highest, but the friction coefficient remains low ($\mu \sim 0.07$). In addition, the top layer that is formed during the first sliding passes for the previously discussed FL films is absent. Further, the low hardness of these films (see Table 1) contributes to their high wear rates.

### *3.3. XPS analysis of unworn and worn surfaces*

In order to evaluate possible structural changes after friction-wear experiments on FL films deposited at $T_S$ = 300 with $P_{N2}$ = 0 mTorr (DLC) and 0.5 mTorr ($CN_x$), an XPS analysis was performed taking spectra on the nine locations as shown in Fig. 1.

Spectra of C1s for both DLC and $CN_x$ films exhibit four contributions (C0-C3), Fig. 5a and b, respectively. For the DLC film, the C0 peak corresponds to $sp^2$ hybridized carbon, the C1 peak has been associated with $sp^3$ hybridized carbon and the C2-C3 peaks correspond to adventitious carbon (C-O and C=O), in agreement with previous reports [18,22,32] for H-free DLC coatings.

In the case of $CN_x$ films, the assignment of the C1s peaks remains a challenge. Recently work by Hellgren *et al.* [48], and previous one by Rodil *et al.* [49], has indicated that the different peaks forming the spectra are due to differences in the number of nitrogen neighbors on the C atoms. Thus, they have assigned the C0 peak to $sp^2$ hybridized carbon. The C1 peak can correspond to $sp^2$ carbon bonded to pyiridinic N on one side and two carbons on the other (>C=N-). The C2 peak can be assigned to $sp^2$ carbon single bonded to graphitic nitrogen and two carbons (≥C-N<), and C3 corresponds to carbonyl groups (>C=O). Previous work has indicated that the C1 peak must be related to $sp^3$ hybridized carbon while C2 resembling $sp^3$ or $sp^2$ hybridized C-N bonds [5,50–52]. A study of the assignment of each peak in the XPS spectrum of carbon nitride films is out of the scope of this work.

In this study we are more interested in taking advantage of the changes in the contributions from C0 and C1. The C1/C0 ratio, i.e., the changes in the area intensities for the nine locations evaluated on DLC and $CN_x$ are displayed in Fig. 5c and d, respectively. The error bars are the uncertainties on the C1/C0 ratio with a confidence of one sigma. Two fits were employed on the C1s spectra, the first it is assuming the same Gaussian for the four peaks (labeled as Fit 1). The second it is assuming the same Gaussian for the first two peaks and another for the 3rd and the 4th peaks (labeled as Fit 2). Table 2 summarizes the peak parameters for Fit 1 and Fit 2.

As seen in Fig. 5, The C1/C0 ratio has a minimum at the location (2,2) in both DLC and $CN_X$ films; this location corresponds to the worn surface. The other neighbor locations correspond to unworn surfaces. It is important to mention that it was difficult to center the spot, for the acquisition of spectra, on the worn area. The complication arises since, as seen in Fig. 4d and e, the samples present swelling instead of typical wear. Thus, although we placed marks during the wear experiments to identify the location (2,2) in the XPS study, we did not rule out the fact that we acquired XPS spectra from unworn areas with a small contribution from the worn region.

The decrease in the ratio C1/C0 could indicate that the sliding of the probe produces structural changes. Nevertheless, wear and surface exposure to the environment can also cause an increase in C0 because the surface is covered with hydrocarbons [48]. However, this possibility is ruled out since the absolute area of peak C1 is affected. Thus, for the case of the DLC film, the decreasing of the C1/C0 ratio with respect to unworn surfaces indicates that the local swelling of material surface observed in Fig. 4d is accompanied by a $sp^3 \rightarrow sp^2$ carbon transformation, in agreement with observation reported by other authors [8–17]. In addition, since the wear test covers only ~42% of the worn area, we expect that the content of the $sp^2$ hybridized carbon (C0) inside the wear tracks is higher than that presented in Fig. 5c.

For the case of the $CN_x$ film, the C0 and C1 peaks have a similar behavior as in DLC film, which indicate that the worn surface has more $sp^2$ hybridized carbon. The C1 peak assigned either to >C=N- or $sp^3$ hybridized carbon decreases for the worn surface. In a first scenario, this would indicate that the swelling observed in Fig. 3e is accompanied by a reduction of >C=N- bonds, while in the second case ($sp^3$ hybridized carbon) could be consequence of $sp^3 \rightarrow sp^2$ carbon transformation. The C2 and C3 do not present significant changes in their area intensities.

Depending on the structural and mechanical properties of the films, we have observed different mechanisms that contribute to differences in wear behavior. Films deposited at $T_S$ = 20 °C and $P_{N2}$ = 0 and 0.5 mTorr, i.e., amorphous carbon and carbon nitride films with hardness of 49 and 30 GPa, respectively, exhibit a notable local swelling during sliding. This local swelling has been explained for ultrananocrystalline diamond (UNCD) coatings under macrotribological tests as a crystalline to amorphous transition accompanied by a notable expansion of the amorphous phase due to an increase in the atomic volume [44]. A rapid saturation of surface dangling bonds helped by $H_2O$ molecules from environment prevents the cold welding with a possible increment of the friction coefficient [44]. Experiments by other authors have indicated that the absence of passivation leads to high friction coefficient, as was observed for DLC [8] films (sliding again sapphire ball in high vacuum conditions) and self-mated UNCD a H-free DLC films under 1% RH [23]. Based on the previous arguments, and the friction-wear behavior of our films, the local swelling observed in Fig. 4a and b for amorphous carbon and carbon nitride films, respectively, and their low friction indicates that there is enough passivation. This leads to a re-hybridization mechanism and formation of a layer rich in $sp^2$ hybridized carbon, i.e., a tribomechanical mechanism followed by a tribochemical one. The localized shear in the formed layer produces cold welding of asperities that suffer separation after necking or even debris formation [17]. Here, the surface of the formed layer has a high density of dangling bonds that are rapidly passivated resulting in a low friction coefficient (0.06–0.07).

FL carbon and carbon nitride films with hardness of 21.8 and 17 GPa, respectively (films deposited at $T_S$ = 300 °C and $P_{N2}$ = 0 and 0.5 mTorr) display local swelling of the film surface throughout wear-friction test associated with a re-hybridization mechanism [17], which follows a cyclic phenomenon that inhibits the wear. The tribological behavior of these FL films is controlled more by tribomechanical than tribochemical processes. The tribological results suggest that these films could find a larger range of applications because they maintain low wear and friction coefficient.

Finally, films deposited at $T_S$ = 20 and 300 °C with a $P_{N2}$ = 5.0 mTorr, having weaker mechanical properties, exhibited a wear mechanism dominated by a tribochemical process, i.e., the surface passivation phenomenon is dominant because they show a low friction coefficient, similar to amorphous and FL films, but have considerable

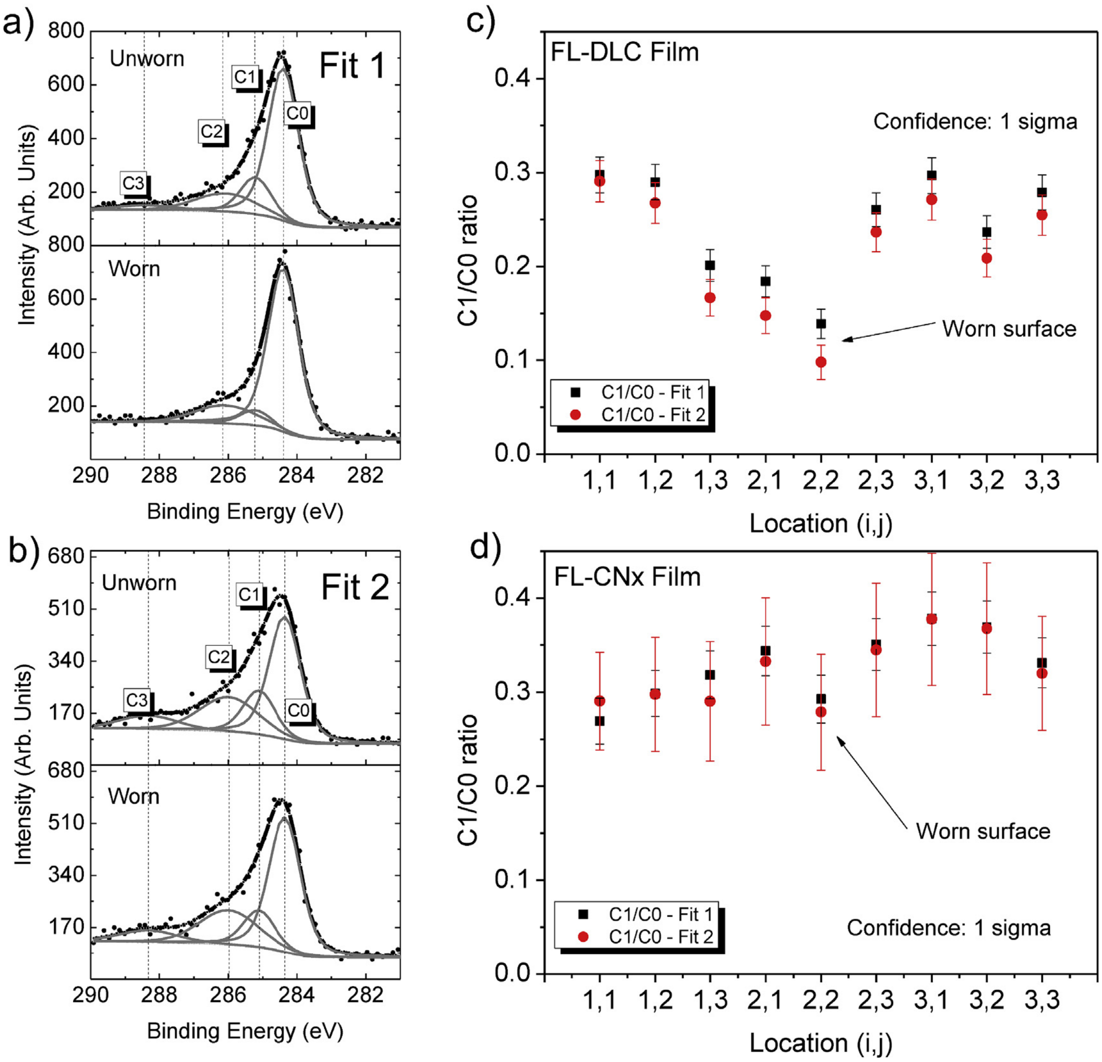

**Fig. 5.** (Color online) Fit of the C1s spectra for unworn and worn surfaces of a) FL-DLC and b) FL-CN$_x$. C1/C0 area ratio from the C1s spectra for c) FL-DLC and d) FL-CN$_x$ films. Fit 1 is assuming the same Gaussian for the four peaks. Fit 2 is assuming the same Gaussian for the first two peaks and another for the 3rd and the 4th peak. Location (2,2) is the worn surface. (For interpretation of the references to colour in this figure legend, the reader is referred to the Web version of this article.)

**Table 2**
Peak parameters for the two fittings presented in Fig. 5c and d.

| Peak parameters for DLC | | | | | | |
|---|---|---|---|---|---|---|
| Component | Energy (eV) | Fit 1 - Peak Width | | Energy (eV) | Fit 2 - Peak Width | |
| | | Gaussian | Lorentzian | | Gaussian | Lorentzian |
| C0 | 284.40 | 0.854 | 0.35 | 284.39 | 0.843 | 0.35 |
| C1 | 285.31 | 0.854 | 0.35 | 285.23 | 0.843 | 0.35 |
| C2 | 286.43 | 0.854 | 0.35 | 286.16 | 1.877 | 0.35 |
| C3 | 287.75 | 0.854 | 0.35 | 288.44 | 1.877 | 0.35 |
| Peak parameters for CN$_x$ | | | | | | |
| Component | Energy (eV) | Fit 1 - Peak Width | | Energy (eV) | Fit 2 - Peak Width | |
| | | Gaussian | Lorentzian | | Gaussian | Lorentzian |
| C0 | 284.40 | 0.961 | 0.35 | 284.35 | 0.880 | 0.35 |
| C1 | 285.40 | 0.961 | 0.35 | 285.10 | 0.880 | 0.35 |
| C2 | 286.50 | 0.961 | 0.35 | 285.98 | 1.773 | 0.35 |
| C3 | 288.12 | 0.961 | 0.35 | 288.32 | 1.773 | 0.35 |

wear.

In brief, after the whole analysis of our experimental results, we can say that the swelling phenomena observed in our experiments is a structural transformation, accompanied by an increase in local volume, mechanically activated (tribomechanical events - re-hybridization).

- For amorphous carbon surfaces with good mechanical properties, the swelling is accompanied by wear debris, which are precursors of the observed wear.
- For FL surfaces with good mechanical properties, there is swelling but the formation of wear debris is much lower than on amorphous surfaces. Furthermore, there is no significant agglomeration of wear debris on the wear track.

## 4. Conclusions

A study of the micro-tribological performance of amorphous and fullerene-like (FL) carbon and carbon nitride coatings deposited by filtered cathodic arc was presented. The tribological results of the films were obtained through a linear reciprocating test using a conical diamond tip as the counterpart subjected to 5 mN applied load under 23 °C temperature and 50% relative humidity. All films have low friction coefficients with values between 0.06 and 0.07 throughout the tribological test; however, they showed different wear mechanisms. Amorphous carbon and carbon nitride films, deposited at a substrate temperature of 20 °C and $N_2$ pressures of 0 and 0.5 mTorr, presented a wear mechanism dominated by tribomechanical events (re-hybridization) rather than tribochemical processes (surface passivation phenomena). Wear results of the amorphous films, produced at substrate temperatures of 20 °C and 300 °C deposited under a $N_2$ pressure of 5 mTorr, indicate that the dominant mechanism is probably dangling bond passivation and, additionally, the low hardness of these films contributes to the highest wear. Films with FL structures, deposited at a substrate temperature of 300 °C and $N_2$ pressures of 0 and 0.5 mTorr, present a swelled layer of material of 3–4 nm thick that is maintained during entire test. The wear results indicate that this swelling material acts like a lubricious layer that inhibits wear and is consequence of a re-hybridization. X-ray photoelectron spectroscopy analysis on virgin and worn surfaces of these FL carbon and carbon nitride films indicates that the lubricious layer, formed during the sliding due to plasticity events induced by localized shear, is rich in $sp^2$ hybridized carbon.

## Acknowledgements

The authors acknowledge the support from the Swedish Government Strategic Research Area in Materials Science on Functional Materials at Linköping University (Faculty Grant SFO Mat LiU No 2009 00971) and the SSF synergy grant FUNCASE. E.B. also acknowledges the partial support from COST Action MP1303 “Understanding and Controlling Nano and Mesoscale Friction.” FJFR acknowledge the support from FOINS - CONACYT Project 2016-01-2488, and the VIEP-BUAP Projects.

## References

[1] Broitman E, Hultman L. Advanced Carbon-Based Coatings, Reference Module in Materials Science and Materials Engineering. Elsevier9780128035818; 2016https://doi.org/10.1016/B978-0-12-803581-8.09211-0.

[2] Berlind T, Furlan a, Czigany Z, Neidhardt J, Hultman L, Arwin H. Spectroscopic ellipsometry characterization of amorphous carbon and amorphous, graphitic and fullerene-like carbon nitride thin films. Thin Solid Films 2009;517:6652–8. https://doi.org/10.1016/j.tsf.2009.04.065.

[3] Fontaine J. Towards the use of diamond-like carbon solid lubricant coatings in vacuum and space environments. Proc Inst Mech Eng Part J J Eng Tribol 2008;222:1015–29. https://doi.org/10.1243/13506501JET323.

[4] Neidhardt J, Hultman L, Broitman E, Scharf TW, Singer IL. Structural, mechanical and tribological behavior of fullerene-like and amorphous carbon nitride coatings. Diam Relat Mater 2004;13:1882–8. https://doi.org/10.1016/j.diamond.2004.05.012.

[5] Flores-Ruiz FJ, Enriquez-Flores CI, Chiñas-Castillo F, Espinoza-Beltrán FJ. Nanotribological performance of fullerene-like carbon nitride films. Appl Surf Sci 2014;314:193–8. https://doi.org/10.1016/j.apsusc.2014.06.168.

[6] Hellgren N, Johansson MP, Broitman E, Hultman L, Sundgren J. Role of nitrogen in the formation of hard and elastic $CN_x$ thin films by reactive magnetron sputtering. Phys Rev B 1999;59:5162–9.

[7] Amaratunga GAL, Chhowalla M, Kiely CJ, Alexandrou I, A R, Devenish RM. Hard elastic carbon thin films from linking of carbon nanoparticles. Nature 1996;383:321.

[8] Voevodin AA, Phelps AW, Zabinski JS, Donley MS. Friction induced phase transformation of pulsed laser deposited diamond-like carbon. Diam Relat Mater 1996;5:1264–9. https://doi.org/10.1016/0925-9635(96)00538-9.

[9] Erdemir A, Bindal C, Fenske GR, Zuiker C, Wilbur P. Characterization of transfer layers on steel surfaces sliding against diamond-like carbon hydrocarbon films in dry nitrogen. Surf Coating Technol 1995;76–77:559–63. https://doi.org/10.1016/S0257-8972(96)03073-3.

[10] Erdemir A, Bindal C, Fenske GR, Zuiker C, Wilbur P. Characterization of transfer layers forming on surface sliding again diamond -like carbon. Surf Coating Technol 1996;86–87:692–7.

[11] Tambe N, Bhushan B. Nanoscale friction-induced phase transformation of diamond-like carbon. Scripta Mater 2005;52:751–5. https://doi.org/10.1016/j.scriptamat.2004.12.013.

[12] Joly-Pottuz L, Matta C, De Barros Bouchet MI, Vacher B, Martin J-MM, Sagawa T, et al. Superlow friction of ta-C lubricated by glycerol: an electron energy loss spectroscopy study. J Appl Phys 2007;102:64912. https://doi.org/10.1063/1.2779256.

[13] M'ndange-Pfupfu A, Eryilmaz O, Erdemir A, Marks LD. Quantification of sliding-induced phase transformation in N3FC diamond-like carbon films. Diam Relat Mater 2011;20:1143–8. https://doi.org/10.1016/j.diamond.2011.06.028.

[14] Merkle AP, Erdemir A, Eryilmaz OL, Johnson JA, Marks LD. In situ TEM studies of tribo-induced bonding modifications in near-frictionless carbon films. Carbon N Y 2010;48:587–91. https://doi.org/10.1016/j.carbon.2009.08.036.

[15] Ma T-B, Wang L-F, Hu Y-Z, Li X, Wang H. A shear localization mechanism for lubricity of amorphous carbon materials. Sci Rep 2014;4:3662. https://doi.org/10.1038/srep03662.

[16] Pastewka L, Moser S, Gumbsch P, Moseler M. Anisotropic mechanical amorphization drives wear in diamond. Nat Mater 2011;10:34–8. https://doi.org/10.1038/nmat2902.

[17] Kunze T, Posselt M, Gemming S, Seifert G, Konicek AR, Carpick RW, et al. Wear, plasticity, and rehybridization in tetrahedral amorphous carbon. Tribol Lett 2014;53:119–26. https://doi.org/10.1007/s11249-013-0250-7.

[18] Flores-Ruiz FJ, Herrera-Gomez A, Camps E, Espinoza-Beltrán FJ. Elastic heterogeneities at the nanoscale in DLC films grown by PLD. Mater Res Express 2015;2:25009. https://doi.org/10.1088/2053-1591/2/2/025009.

[19] Wagner H, Bedorf D, Küchemann S, Schwabe M, Zhang B, Arnold W, et al. Local elastic properties of a metallic glass. Nat Mater 2011;10:439–42. https://doi.org/10.1038/nmat3024.

[20] Liu YH, Wang D, Nakajima K, Zhang W, Hirata a, Nishi T, et al. Characterization of nanoscale mechanical heterogeneity in a metallic glass by dynamic force microscopy. Phys Rev Lett 2011;106:125504. https://doi.org/10.1103/PhysRevLett.106.125504.

[21] Broitman E. The nature of the frictional force at the macro-, micro-, and nano-scales. Friction 2014;2:40–6. https://doi.org/10.1007/s40544-014-0037-3.

[22] Jantschner O, Field SK, Holec D, Fian a, Music D, Schneider JM, et al. Origin of temperature-induced low friction of sputtered Si-containing amorphous carbon coatings. Acta Mater 2015;82:437–46. https://doi.org/10.1016/j.actamat.2014.09.030.

[23] Konicek AR, Grierson DS, Sumant AV, Friedmann TA, Sullivan JP, Gilbert PUPA, et al. Influence of surface passivation on the friction and wear behavior of ultra-nanocrystalline diamond and tetrahedral amorphous carbon thin films. Phys Rev B Condens Matter 2012:85. https://doi.org/10.1103/PhysRevB.85.155448.

[24] Broitman E, Flores-Ruiz FJ. Novel method for in-situ and simultaneous nanofriction and nanowear characterization of materials. J Vac Sci Technol A Vacuum, Surfaces, Film 2015;33:43201. https://doi.org/10.1116/1.4921584.

[25] Tucker MD, Czigány Z, Broitman E, Näslund L-Å, Hultman L, Rosen J. Filtered pulsed cathodic arc deposition of fullerene-like carbon and carbon nitride films. J Appl Phys 2014;115:144312. https://doi.org/10.1063/1.4871179.

[26] Broitman E. Indentation hardness measurements at macro-, micro-, and nanoscale: a critical overview. Tribol Lett 2017;65:23. https://doi.org/10.1007/s11249-016-0805-5.

[27] Hysitron TriboIndenter TI-950. 2018https://www.bruker.com/nc/products/surface-and-dimensional-analysis/nanomechanical-test-instruments/standalone-nanomechanical-test-instruments/ti-950-triboindenter/overview.html.

[28] Diliegros-Godines CJ, Flores-Ruiz FJ, Castanedo-Pérez R, Torres-Delgado G, Espinoza-Beltrán FJ, Broitman E. Mechanical and tribological properties of CdO + SnO2 thin films prepared by sol–gel. J Sol Gel Sci Technol 2015;74:114–20. https://doi.org/10.1007/s10971-014-3584-1.

[29] Flores-Ruiz FJ, Diliegros-Godines CJ, Hernández-García FA, Castanedo-Pérez R, Torres-Delgado G, Broitman E. Mechanical and tribological behavior of sol–gel TiO2–CdO films measured at the microscale levels. J Sol Gel Sci Technol 2017. https://doi.org/10.1007/s10971-017-4346-7.

[30] Rivera-Tello CD, Broitman E, Flores-Ruiz FJ, Jiménez O, Flores M. Mechanical properties and tribological behavior at micro and macro-scale of wc/WCN/W hierarchical multilayer coatings. Tribol Int 2016;101:194–203. https://doi.org/10.1016/j.triboint.2016.04.017.

[31] Muñoz-Flores J, Herrera-Gomez A. Resolving overlapping peaks in ARXPS data: the

effect of noise and fitting method. J Electron Spectrosc Relat Phenom 2012;184:533–41. https://doi.org/10.1016/j.elspec.2011.08.004.

[32] Herrera-Gomez A, Sun Y, Aguirre-Tostado, Francisco Servando Hwang C, Mani-Gonzalez PG, Flint E, Espinosa-Magaña F, et al. Structure of ultra-thin diamond-like carbon films grown with filtered cathodic arc on Si (001). Anal Sci 2010;26:267–72.

[33] Herrera-Gomez A. Simultaneous Data Fitting in ARXPS. Cinvestav Unidad Queretaro intern Rep; 2008. p. 1–7http//rdataa.com/aanalyzer/docs/aana/SimultaneousFitting.pdf.

[34] Herrera-Gomez A. AAnalyzer®: a peak-fitting program for photoemission data. http://rdataa.com/aanalyzer/aanaHome.htm; 2017.

[35] Herrera-Gomez A. A rigorous approach to the calculation of the uncertainties in XPS analysis Internal Report. CINVESTAV-Unidad Queretaro http://www.qro.cinvestav.mx/~aherrera/reportesInternos/uncertaintiesXPS.pdf; 2017.

[36] Herrera-Gomez A, Porter RM. Mixed linear-nonlinear least squares regression vol. 10. 2017. p. 1–17. arXiv:170304181v1.

[37] Andersson J, Erck RA, Erdemir A. Frictional behavior of diamondlike carbon films in vacuum and under varying water vapor pressure. Surf Coating Technol 2003;163–164:535–40. https://doi.org/10.1016/S0257-8972(02)00617-5.

[38] Villarrubia JS. Algorithms for scanned probe microscope image simulation, surface reconstruction, and tip estimation. J Res Natl Inst Stand Technol 1997;102:425. https://doi.org/10.6028/jres.102.030.

[39] Flater EE, Zacharakis-Jutz GE, Dumba BG, White IA, Clifford CA. Towards easy and reliable AFM tip shape determination using blind tip reconstruction. Ultramicroscopy 2014;146:130–43. https://doi.org/10.1016/j.ultramic.2013.06.022.

[40] Anders A, Ieee F, Fong W, Kulkarni A, Ryan FW, Bhatia CS. Ultrathin diamond-like carbon films deposited by filtered carbon vacuum arcs ultrathin diamond-like carbon films deposited by filtered carbon vacuum arcs. IEEE Trans Plasma Sci 2001;29:1–21.

[41] Drescher D, Koskinen J, Scheibe H-J, Mensch A. A model for particle growth in arc deposited armophous carbon films. Diam Relat Mater 1998;7:1375–80. https://doi.org/10.1016/S0925-9635(98)00211-8.

[42] Nečas D, Klapetek P. Gwyddion: an open-source software for SPM data analysis. Cent Eur J Phys 2012;10:181–8. https://doi.org/10.2478/s11534-011-0096-2.

[43] Bakoglidis K, Glenat H, Greczynsky G, Schmidt S, Grillo S, Hultman L, Broitman E. Comparative study of macro- and microtribological properties of carbon nitride thin films deposited by HiPIMS. Wear 2017;370–371:1–8.

[44] De Barros Bouchet MI, Matta C, Vacher B, Le-Mogne T, Martin JM, von Lautz J, et al. Energy filtering transmission electron microscopy and atomistic simulations of tribo-induced hybridization change of nanocrystalline diamond coating. Carbon N Y 2015;87:317–29. https://doi.org/10.1016/j.carbon.2015.02.041.

[45] Broitman E, Neidhardt J, Hultman L. Fullerene-like carbon nitride: a new carbon-based tribological coating. Tribol. Diamond-Like Carbon Film. Fundam. Appl 2008:620–53. https://doi.org/10.1007/978-0-387-49891-1_24.

[46] Kracica M, Kocer C, Lau DWM, Partridge JG, Bradby JE, Haberl B, et al. The mechanical properties of energetically deposited non-crystalline carbon thin films. Carbon N Y 2016;98:391–6. https://doi.org/10.1016/j.carbon.2015.10.085.

[47] Broitman E, Gueorguiev GK, Furlan A, Son NT, Gellman AJ, Stafström S, et al. Water adsorption on fullerene-like carbon nitride overcoats. Thin Solid Films 2008;517:1106–10. https://doi.org/10.1016/j.tsf.2008.07.022.

[48] Hellgren N, Haasch RT, Schmidt S, Hultman L, Petrov I. Interpretation of X-ray photoelectron spectra of carbon-nitride thin films: new insights from in situ XPS. Carbon N Y 2016;108:242–52. https://doi.org/10.1016/j.carbon.2016.07.017.

[49] Rodil SE, Morrison N a, Robertson J, Milne WI. Nitrogen incorporation into tetrahedral hydrogenated amorphous carbon. Phys Status Solidi 1999;174:25–37. https://doi.org/10.1002/(SICI)1521-396X(199907)174. 1 < 25::AID-PSSA25 > 3.0.CO;2–3.

[50] Roy SS, McCann R, Papakonstantinou P, Maguire P, McLaughlin JA. The structure of amorphous carbon nitride films using a combined study of NEXAFS, XPS and Raman spectroscopies. Thin Solid Films 2005;482:145–50. https://doi.org/10.1016/j.tsf.2004.11.132.

[51] Hellgren N, Guo J, Luo Y, Såthe C, Agui A, Kashtanov S, et al. Electronic structure of carbon nitride thin films studied by X-ray spectroscopy techniques. Thin Solid Films 2005;471:19–34. https://doi.org/10.1016/j.tsf.2004.03.027.

[52] Bakoglidis KD, Schmidt S, Garbrecht M, Ivanov IG, Jensen J, Greczynski G, et al. Low-temperature growth of low friction wear-resistant amorphous carbon nitride thin films by mid-frequency, high power impulse, and direct current magnetron sputtering. J Vac Sci Technol A Vacuum, Surfaces, Film 2015;33. https://doi.org/10.1116/1.4923275. 05E112.